J Mater Sci (2010) 45:575–581
DOI 10.1007/s10853-009-3929-2

Densification of porous 8 mol% yttria-stabilized zirconia component: modelling and experimental studies

J. Lu · X. C. Song · T. S. Zhang · H. H. Hng · J. Ma

Received: 26 April 2009 / Accepted: 24 September 2009 / Published online: 8 October 2009

Abstract In this paper, the densification of a ceramic powder matrix that contained large macropores of the size much larger than the average grain size of the matrix was studied. The grain-boundary diffusion controlled sintering models of ceramic matrix contained large macropores were first established. A sintering potential associated with the macropores was also verified and introduced into the models. The experimental data were collected for the sintering of porous 8 mol% yttria-stabilized zirconia system with 20 vol% large pores. The predictions of the model were found in good agreement with experimental data.

Introduction

An increasing number of porous ceramics were applied to various advanced applications including electrodes of Solid Oxide Fuel Cells (SOFCs), high-temperature thermal insulation, support for catalytic reactions, filters and membranes for high-temperature gas cleaning or molten metal filtration, and gas burner media, etc. The performance of these ceramics depends on their structure parameters including porosity and, pore size etc. However, the porosity introduced from the initial powder compaction is not enough to fulfill the generally accepted levels of porosity for the advanced porous ceramic applications. Additional porosity can be achieved using artificial pore formers. The size of the pores left by the pore formers can be much bigger than the average grain size. In this paper, situation where the pore diameter is much larger than the average grain size will be defined as 'macropore' and 'micropore' refers to where the pore diameter is approximately the same or smaller than the grain size. During the early stage of sintering, micropores can be sintered quickly and disappear. However, the macropores are much larger and may even grow. Hence, the interaction between these macropores and matrix will be different from that of micropores, and will have a huge effect to the densification of ceramic components. As a result, the sintering characteristics of the macropores need to be studied separately from those of micropores.

Since Frenkel first proposed a model for the sintering of viscous materials in 1945, constitutive models have been wildly used to evaluate sintering parameters, describe the densification and grain growth process, and identify the sintering mechanism of porous bodies. However, in most constitutive models, the pore is mainly in the range of micropores. Lange et al. [1–3] have reported in their earlier work that during the sintering process, a pore can only shrink if it has a coordination number which is lower than the critical coordination number. In a later work, Slamovich and Lange [4, 5] observed that the shrinkage behaviours of large pores were not controlled by coordination number, but by the characteristic diffusion distance. However, in the situation where the size of pores is much larger than the mean grain size, Cocks and Searle [6] found that the shrinkage of large pores was not from the direct diffusion from matrix to pores, but resulted from the deformation of surrounding grains. By combining the large amount of experimental data on porous body densification, Cocks [7]

J. Lu (✉) · X. C. Song · H. H. Hng · J. Ma
School of Materials Science and Engineering, Nanyang Technological University, Singapore 639798, Singapore
e-mail: luji0004@ntu.edu.sg

T. S. Zhang
Institute of Materials Research and Engineering (IMRE), Singapore 117602, Singapore

J. Ma
Temasek Laboratories, Nanyang Technological University, 50 Nanyang Drive, Singapore 637553, Singapore

proposed that sintering potential only depends on the size of the pores and the sintering behaviours of the micropores and macropores have to be considered separately. This idea is supported by the numerical study of Pan et al. [8].

In present work, the relationship of sintering controlled by grain-boundary diffusion mechanism for macroporous ceramic component was studied. In this model, unlike the classical approaches, the sintering potential of large macropores was introduced separately from that of fine micropores in an interconnected porous network system.

Materials modelling

Figure 1 shows the material system for the present work. The size of large macropores is much bigger than the average grain size of the microporous matrix (which means the pore size in the matrix is mainly of the order of the average grain size or smaller). This porous body is subjected to a stress Σ_{ij} and creeps at a rate $\dot{E}_{ij}$.

The linear grain-boundary diffusion models will be applied as grain-boundary diffusion is well accepted to be the dominant mechanism for fine-grained body sintering. The grain-boundary diffusion constitutive law can be generally written as

$$\dot{\varepsilon}_{ij} = \frac{1}{2\mu} s_{ij} + \frac{1}{3\kappa}\sigma_m \delta_{ij} \tag{1}$$

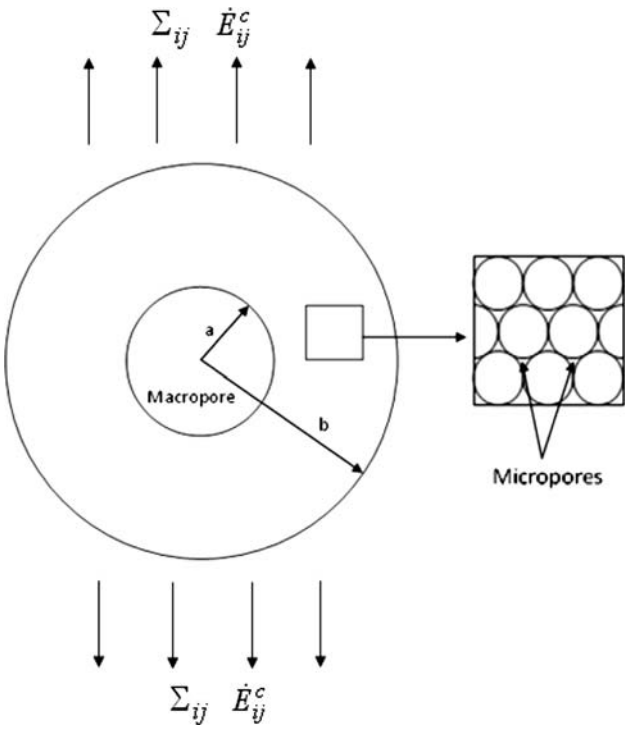

Fig. 1 A material system of macropore of radius "a" surrounded by a microporous matrix with a mean spacing "$2b$"

where $\dot{\varepsilon}_{ij}$ is the strain rate, S_{ij} and σ_m are deviatoric stress tensor and mean stress, respectively; while δ_{ij} is the Kroneker delta, μ is the shear viscosity and κ is the bulk viscosity. μ and κ satisfy the relationship [9, 10]:

$$\mu = \frac{\frac{\sigma_0}{\dot{\varepsilon}_0}\left(\frac{L}{L_0}\right)^3}{3c(\rho)} \tag{2}$$

$$\kappa = \frac{\frac{\sigma_0}{\dot{\varepsilon}_0}\left(\frac{L}{L_0}\right)^3}{9f(\rho)} \tag{3}$$

where $\dot{\varepsilon}_0$ is the uniaxial strain rate at a given stress σ_0 for a fully dense material of grain size L_0, $f(\rho)$ and $c(\rho)$ are dimensionless functions of the relative density.

For macroporous material system, the situation will be more complicated. The macroporous system can be considered as a composite system containing two parts: a microporous matrix and macropores that are much larger than the average grain size. Ignoring the interactions between the macropores, the strain rate of a macroporous system can be expressed using Eshelby's expressions [11] as:

$$\dot{\varepsilon}_{ij} = \frac{\sigma_m \delta_{ij}}{2\mu(1+v)}\left[(1-2v) + \frac{3}{2} f_v (1-v)\right] + \frac{s_{ij}}{2\mu(7-5v)}[(7-5v) + 15 f_v (1-v)] \tag{4}$$

where v is Poisson's ratio, and f_v is volume fraction of the large pores.

In above equation, the volumetric strain rate is mainly due to the mean stress σ_m. However, in practice, both micro and macropores will shrink during the sintering even without externally loaded stress. Thus, the sintering potentials of micro and macropores should both be introduced to the models.

For situations where different mechanisms are involved, it is proved convenient to introduce the strain rate potential and stress potential, which are related as follows:

$$\sigma_{ij}\dot{\varepsilon}_{ij} = \phi + \varphi \tag{5}$$

where ϕ is a function of stress and φ is a function of strain rate. The stress σ_{ij} and strain rate $\dot{\varepsilon}_{ij}$ at a material point can then be determined from the stress potential and strain rate potential, respectively, in the following manner:

$$\dot{\varepsilon}_{ij} = \frac{\partial \varphi}{\partial \sigma_{ij}};\ \sigma_{ij} = \frac{\partial \phi}{\partial \dot{\varepsilon}_{ij}} \tag{6}$$

The situation where a porous body subjected to a stress Σ_{ij} and creeps at a rate $\dot{E}_{ij}$ is considered, an element of material within a grain experiences a stress σ_{ij}. The total volume of the porous body is V, the volume of the microporous matrix is V_m, $V-V_m$ gives the volume of the large pores. The body has a surface area A_s and grain boundaries of total area A_b.

Following the expression proposed by Cocks [12] where the convexity condition was used

$$\Phi \geq \Sigma_{ij}\dot{E}_{ij} - \Psi^c \tag{7}$$

where

$$\Psi^c = \frac{1}{V}\left[\int_{V_m} \psi^c \mathrm{d}V + \gamma_s \dot{A}_s^c + \gamma_b \dot{A}_b^c\right] \tag{8}$$

$\dot{A}_s^c$ and $\dot{A}_b^c$ are the rates of change of surface and boundary area and the superscript c represents an assumed compatible strain rate field within the macroscopic element. The first term of right part comes from the microporous matrix, and the last two arise from the macropores.

Before introducing the sintering potentials to the models, the stresses of a macropore experiencing hydrostatic stresses in a microporous matrix will be first analyzed by a thick-walled hollow shell.

Figure 2a shows the cross section of a macropore with its surrounding microporous matrix, where a is the macropore radius and b is half of the mean spacing between the macropores. The body is subjected to a uniform external pressure, σ_m, and the principal stresses are σ_r, σ_ϕ, σ_θ shown in Fig. 2b.

The thick-walled shell analysis demonstrates that the macroscopic volumetric strain rate is from two fields: dilatational and deviatoric fields.

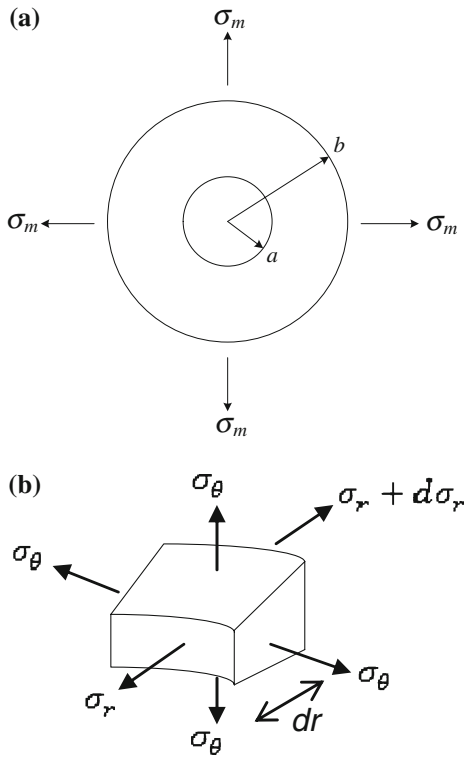

Fig. 2 **a** Cross section of the spherical shell **b** principal stresses acting on an element

For the dilatational part:

$$\dot{\varepsilon}_r = \dot{\varepsilon}_\phi = \dot{\varepsilon}_\theta = A \tag{9}$$

$$\dot{\varepsilon}_m = \frac{1}{3}(\dot{\varepsilon}_r + \dot{\varepsilon}_\phi + \dot{\varepsilon}_\theta) = A \tag{10}$$

and for the deviatoric part:

$$\dot{\varepsilon}_r = -2\dot{\varepsilon}_\phi = -2\dot{\varepsilon}_\theta = -\frac{2B}{r^3} \tag{11}$$

where r is the radial distance from the centre of the cell. A and B represent the magnitudes of the two fields. The macroscopic volumetric strain rate can be obtained by combining these two fields:

$$\dot{E}_{kk} = 3\left(A + \frac{B}{b^3}\right) \tag{12}$$

Then, the sintering potentials will be introduced to the models.

The stress potential for the microporous matrix (the first term of right part of Eq. 8) of the situation where a sintering potential operates can be expressed as:

$$\frac{1}{V}\int_{V_m} \psi^c \mathrm{d}V = \frac{1}{V}\left(\int_{V_m} \psi \mathrm{d}V + \int_{V_m} \sigma_{s\rho}\dot{\varepsilon}_{kk}\mathrm{d}V\right)$$

and

$$\psi = \frac{3}{2}\mu\dot{E}_e^2 + \frac{9}{2}\kappa\dot{E}_m^2 \tag{13}$$

where $\sigma_{s\rho}$ is the sintering potential associated with the micropores.

In the case of macroporous body, when the large pores shrink during the sintering, the surrounding materials will experience superplastic deformation, i.e., the grains simply rearrange, and the total area of grains remains constant [7]. If the surface area of the pores increased by an amount of $\dot{A}_s^c$, this will be accompanied by a decrease in the grain-boundary area of an amount of $\dot{A}_b^c$ which equals to $-1/2\dot{A}_s^c$.

The rate of change of surface area of the macropore can be expressed in terms of the field quantities A and B:

$$\dot{A}_s = 8\pi a\left(Aa + \frac{B}{a^2}\right) \tag{14}$$

Then,

$$\gamma_s\dot{A}_s^c + \gamma_b\dot{A}_b^c = \left(\gamma_s - \frac{1}{2}\gamma_b\right)\cdot 8\pi a^2\left(A + \frac{B}{a^3}\right) \tag{15}$$

Combine Eq. 8 to (15) with (7) gives

$$\Phi = 3\Sigma_m\left(A + \frac{B}{b^3}\right) - 6\mu B^2\frac{(1-f_v)}{a^3b^3} - \frac{9\kappa}{2}A^2(1-f_v) - 3\sigma_{s\rho}(1-f_v)A - 3f_v\sigma_{sR}\left(A + \frac{B}{b^3}\right) \tag{16}$$

where

$$\sigma_{sR} = \frac{2\gamma_s}{a}\left(1 - \frac{\gamma_b}{2\gamma_s}\right) \tag{17}$$

is the sintering potential associated with the macropores. It is related to the size of the large macropores and influenced by the surface and grain-boundary energies.

f_v is volume fraction of the large pores, a^3/b^3.

Optimizing Eq. 16 with respect to A and B, we can have

$$A = \frac{\Sigma_m - \sigma_{s\rho}(1-f_v) - \sigma_{sR}f_v}{3\kappa(1-f_v)} \tag{18}$$

$$B = \frac{3(\Sigma_m - \sigma_{sR})f_v b^3}{12\mu(1-f_v)} \tag{19}$$

Finally by substituting A and B back into (16) and combining with the deviatoric strain rate term by Eshelby (Eq. 4), the full expression for the strain rate potential is:

$$\Phi = \frac{1}{2\mu_n}\Sigma_e^2 + \frac{1}{2\kappa}\frac{\left[\Sigma_m - \sigma_{s\rho}(1-f_v) - \sigma_{sR}f_v\right]^2}{1-f_v} + \frac{3}{8\mu}\frac{(\Sigma_m - \sigma_{sR})^2 f_v}{1-f_v} \tag{20}$$

with $\mu_n = \mu\frac{7-5\upsilon}{(7-5\upsilon)+15f_v(1-\upsilon)}$ using $\dot{\varepsilon}_{ij} = \frac{\partial\phi}{\partial\sigma_{ij}}$ [12], the strain rate expression for grain-boundary diffusion controlled sintering is:

$$\dot{E}_{ij} = \frac{S_{ij}}{2\mu(7-5\upsilon)}[(7-5\upsilon) + 15f_v(1-\upsilon)] + \frac{1}{3\kappa}\frac{\Sigma_m - \sigma_{s\rho}(1-f_v) - \sigma_{sR}f_v}{1-f_v} + \frac{1}{4\mu}\frac{(\Sigma_m - \sigma_{sR})f_v}{1-f_v} \tag{21}$$

The densification rate can be determined as

$$\dot{\rho} = -\rho\dot{\varepsilon}_v \tag{22}$$

We can now obtain the densification rate equation from Eqs. 21 and 22:

$$\dot{\rho} = \rho\left[\frac{-3S_{ij}}{2\mu(7-5\upsilon)}[(7-5\upsilon) + 15f_v(1-\upsilon)] - \frac{1}{\kappa}\frac{\Sigma_m - \sigma_{s\rho}(1-f_v) - \sigma_{sR}f_v}{1-f_v} - \frac{3}{4\mu}\frac{(\Sigma_m - \sigma_{sR})f_v}{1-f_v}\right] \tag{23}$$

In Eq. 23, the sintering potential associated with microporous matrix $\sigma_{s\rho}$ and dimensionless function $f(\rho)$ is chosen based on the work of Du and Cocks [9]

$$\sigma_{s\rho} = \frac{4.5\gamma_s}{L}\rho^2\left(\frac{2\rho - \rho_0}{1-\rho_0}\right) \tag{24}$$

$$f(\rho) = \frac{0.54(1-\rho_0)^2}{\rho(\rho-\rho_0)^2} \tag{25}$$

After substituting Eqs. 24, 25 and 17 of σ_{sR} into Eq. 23, the densification rate equation contains the relative density, grain size, macropore diameter and volume fraction of large pores as variables, which can be obtained directly from experiments. And when the volume fraction of large pores, f_v, equals to zero, Eq. 23 will reduce to the original form for a homogenous microporous body.

Experimental procedure

Raw materials

In present work, commercial 8 mol% yttria-stabilized zirconia (8YSZ) powder (Tosoh, Japan) was used as raw material. The mean particle size of 8YSZ was 0.1 μm. Poly (methyl methacrylate), PMMA microspheres (Struers, Singapore) were added to 8YSZ powders to produce macroporous system. The PMMA was 20% by volume relative to 8YSZ powder. The PMMA microspheres were sieved before the usage, and the mean particle size was between 50 and 70 μm.

Processing

A two-roll milling compaction process was applied to fabricate macroporous 8YSZ. For a better comparison, microporous 8YSZ (without macropores) was also fabricated. Initially a dough was made by weighing out the 8YSZ/PMMA powders, methylcellulose, glycerol and distilled water. The well mixed dough was then rolled on a two-roll-mill until a moist tape was obtained. The tape was then removed from the machine and cut into 15 × 15 mm^2.

Sintering and characterization

The macro- and microporous 8YSZ samples were heated to 150 °C at a heating rate of 25 °C per hour. The samples were held for 1 h to get rid of all the water in the samples. They were then heated to 600 °C at a heating rate of 60 °C per hour, and held for 1 h to eliminate the polymers. The green density of the samples was measured only after the polymers had been burnt out. Then, the samples were heated to 1350 °C at a heating rate of 200 °C per hour, and held for different holding times: 15, 30 min, 1 and 2 h.

The density of the sintered samples D_{measured} was calculated directly by measuring their mass and volume. The relative density ρ was obtained by:

$$\rho = \frac{D_{\text{measured}}}{D_{\text{theoretical}}} \tag{26}$$

where $D_{\text{theoretical}}$ of 8YSZ was taken as 5.95 g/cm^3.

Cross-section images of both microporous and macroporous systems were obtained using a JSM-6340F scanning

electron microscope (SEM, JEOL Company, Japan) after polishing and thermal etching of the samples.

The grain size was determined by counting the number of grains traversed by straight lines. About 150–200 grains were measured for each sample. The final mean grain size was obtained as 1.56 times the average intercept length. The size of the large pores was also measured. About 100–200 pores were measured to obtain the mean pore size. The volume fraction of large pores, f_v, in the overall macroporous body can be written as (see Appendix):

$$f_v = 1 - \left(1 + \frac{1-\rho_m}{\rho_m}\right)\rho \tag{27}$$

where ρ_m is the density of the microporous matrix of the macroporous body, and can be obtained from the SEM images of the cross section of the specimens. ρ is the relative density of the overall macroporous body.

Results and discussion

Sintering results

The SEM images of typical sintered 8YSZ samples are shown in Fig. 3.

SEM image of macroporous sample showed that the large pores dispersed randomly in the microporous 8YSZ matrix.

As stated, the relative densities of sintered samples were calculated, and the grain sizes of sintered samples as well as the large pore sizes of the macroporous samples were measured from SEM images. The results were plotted as functions of time in Fig. 4.

During the experiments, the grain sizes of microporous and macroporous system increased from 0.1 μm to 1.9 and 1.2 μm, respectively. Stage 1 was observed throughout the experiments. And the large pores were found to be shrinking continuously during the sintering process.

The experimental results obtained were used to evaluate the model developed in present work.

Modelling results

For free sintering, there is no external stress applied on the samples, i.e. the mean stress σ_m and deviatoric stress S_{ij} are zero. Hence, the densification rates for macroporous and microporous systems under grain-boundary diffusion are:

$$\dot{\rho}_{\text{macro}} = 9\rho\frac{\dot{\varepsilon}_{0b}}{\sigma_o}\left(\frac{L_0}{L}\right)^3 f_b(\rho)\left[\frac{2\sigma_{s\rho}(1-f_v)+3\sigma_{sR}f_v}{2(1-f_v)}\right] \tag{28}$$

Following Du and Cocks [9], the σ_0 in Eq. 28 can be expressed as $\sigma_0 = \gamma_s/L_0$, the densification rate can then be expressed by

$$\dot{\rho}_{\text{macro}} = 9\rho\dot{\varepsilon}_{0b}\left(\frac{L_0}{\gamma_s}\right)\left(\frac{L_0}{L}\right)^3 f(\rho)\left[\frac{2\sigma_{s\rho}(1-f_v)+3\sigma_{sR}f_v}{2(1-f_v)}\right] \tag{29}$$

In present work, the programming language Java was used to perform the modelling. A simple Euler scheme was adopted to calculate the relative density after a time step, Δt,

$$\rho_{t+\Delta t} = \rho_t + \dot{\rho}_t\Delta t \tag{30}$$

During the modelling, the grain size, diameter of the macropores and volume fraction of the large pores were converted to the function of the relative density in order to avoid added complication. The strain rate constant $\dot{\varepsilon}_{0b}$ cannot be chosen directly, but will be obtained from the modelling process.

The densification behaviours of the microporous and macroporous 8YSZ sintered at 1350 °C were calculated using Eq. 21 ($f_v = 0$ for microporous 8YSZ system), and the results were shown in Fig. 5. The porous model without sintering potential of macropores (σ_{sR}) was also applied to predict the densification of 8YSZ/20% macroporous system using the same modelling parameter. For a better comparison, the experimental data were also plotted in the figure. It was found that the models developed in present work can provide a good agreement between theoretical prediction and experiments. However,

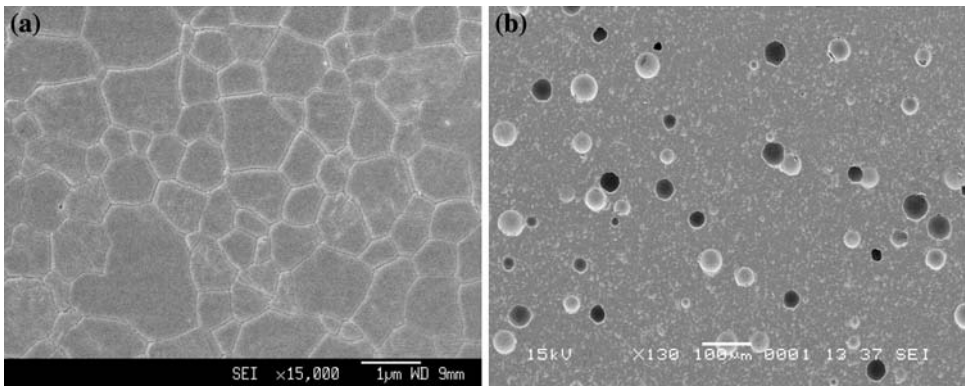

Fig. 3 Microstructures of micro- and macroporous samples sintered at 1350 °C. **a** Microporous sample sintered at 1350 °C for 30 min and **b** macroporous sample sintered at 1350 °C for 1 h

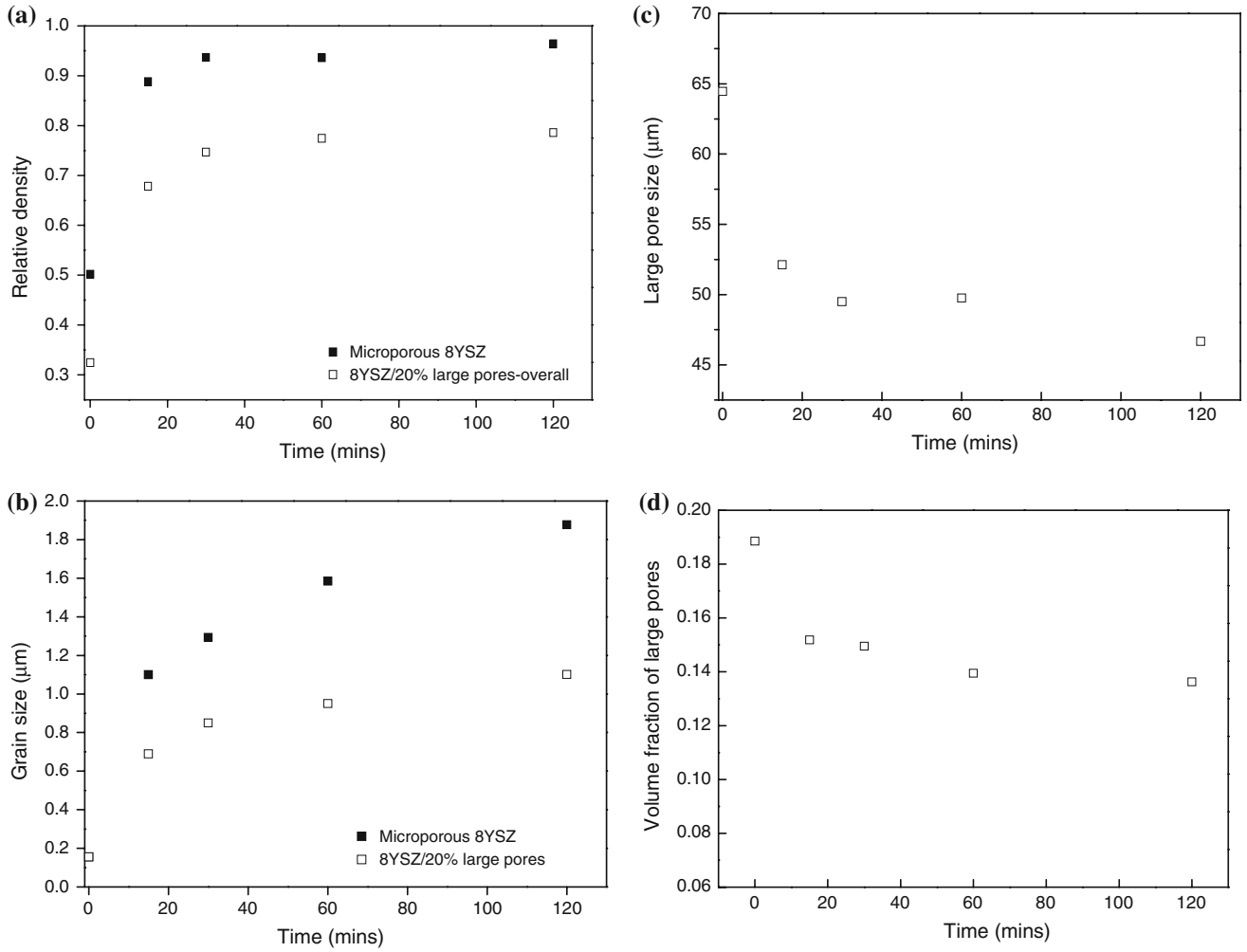

Fig. 4 **a** Relative density of samples sintered at 1350 °C. **b** Grain growth of samples sintered at 1350 °C. **c** Macropore diameter (μm) variation of macroporous 8YSZ sintered at 1350 °C. **d** Volume fraction of large pores (fv) development of macroporous 8YSZ during sintering at 1350 °C (*solid symbol* microporous 8YSZ, *open symbol* 8YSZ/20% large pores)

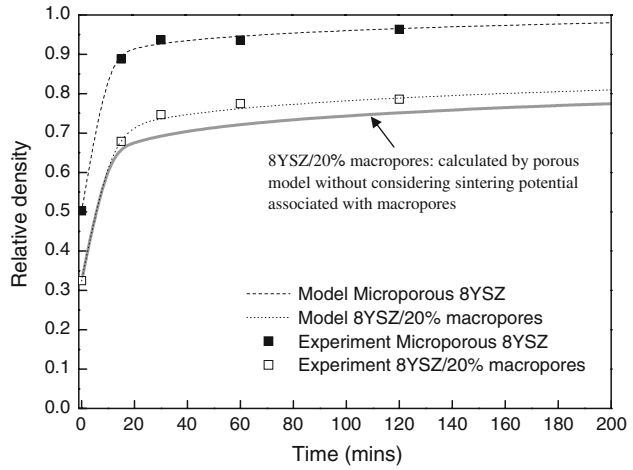

Fig. 5 Modelling results of densification process of sintering at 1350 °C (*solid symbol* microporous 8YSZ, *open symbol* 8YSZ/20% large pores)

the model without σ_{sR} underestimated the densification behaviours of the 8YSZ/20% macroporous system. The reason is that during the sintering, both micro and macropores will shrink. The shrinkage of the macropores provides an additional driving force for the densification of porous body. The introducing of sintering potential associated with the macropores can give a more appropriate description of internal stress state of porous materials. The strain rate constant, $\dot{\varepsilon}_{0b}$ determined as $1.38 \times 10^{-4}\ s^{-1}$ from the modelling process.

The theoretical prediction of the variation of relative density with time for the microporous matrix of 8YSZ/20% macropores was also calculated using Eq. 21 (when $f_v = 0$). And the result is shown in Fig. 6. It can be seen that the theoretical results agreed well with the experimental data. And this result was basically identical to that of the microporous 8YSZ. It showed that in a macroporous

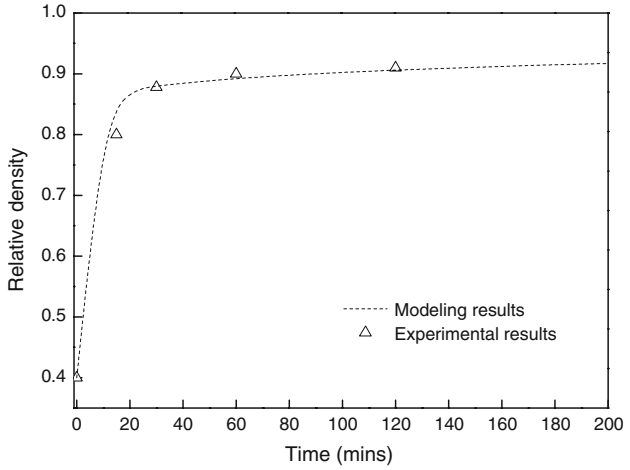

Fig. 6 Modelling results of densification process of microporous matrix of sintering at 1350 °C

material, the microporous matrix still behaved as a homogeneous microporous material.

Conclusions

Models for determining grain-boundary diffusion controlled sintering characteristics of a macroporous body were studied. The expression for the sintering potential associated with macropores was verified, and was introduced separated from the sintering potential of fine micropores. The theoretical prediction of macroporous material densification gave good and more reasonable agreement to experimental results comparing to the microporous model.

Our model is one of the very few models that separate macropores from micropores, and the results indicated that by introducing the sintering potential associated with the macropores, the constitutive model gave a more accurate prediction of densification of porous materials that consists of both micro- and macropores.

Appendix. Volume fraction of large pores in a macroporous system

The density of the overall macroporous body, ρ, can be obtained by measuring the volume and mass of the samples, and can be written as

$$\rho = \frac{V_d}{V_{bp} + V_{sp} + V_d} \tag{31}$$

where V_d is the volume of the dense part, V_{bp} is the volume of the large pores and V_{sp} is the volume of the small micropores.

The density of the microporous matrix in the macroporous system, ρ_m, can be expressed as

$$\rho_m = \frac{V_d}{V_{sp} + V_d} \tag{32}$$

ρ_m can be obtained from the SEM micrographs of the cross section of the specimens.

The volume fraction, f_v, of the large macropores can be expressed as

$$f_v = \frac{V_{bv}}{V_{sp} + V_d + V_{bp}} \tag{33}$$

From Eqs. 31 and 32, Eq. 33 can be expressed in terms of ρ and ρ_m as

$$f_v = 1 - \left(1 + \frac{1 - \rho_m}{\rho_m}\right)\rho \tag{34}$$

References

1. Lange FF (1984) J Am Ceram Soc 67:83
2. Kellett BJ, Lange FF (1989) J Am Ceram Soc 72:725
3. Lange FF, Kellett BJ (1989) J Am Ceram Soc 72:735
4. Slamovich EB, Lange FF (1992) J Am Ceram Soc 75:2498
5. Slamovich EB, Lange FF (1993) J Am Ceram Soc 76:1584
6. Cocks ACF, Searle AA (1991) Mech Mater 12:279
7. Cocks ACF (2001) Prog Mater Sci 46:201
8. Pan J, Ch'ng HN, Cocks ACF (2005) Mech Mater 37:705
9. Du ZZ, Cocks ACF (1992) Acta Metall Mater 40:1969
10. Du ZZ, Cocks ACF (1992) Acta Metall Mater 40:1981
11. Eshelby JD (1961) In: Sneddon I, Hill R (eds) Progress in solid mechanics. Interscience, New York
12. Cocks ACF (1994) Acta Metall Mater 42:2191